# The robust pipe thinning detection method using high precision distributed fiber sensing

A. GUZIK, Y. YAMAUCHI, K. KISHIDA, C-H LI

## ABSTRACT

The paper deals with the thinning detection method, utilizing the *Neubrescope* optical fiber sensing system. The repeatability and reliability of measurements are examined in detail. The influence of polarization average, frequency-scanning step, as well as self-calibration is studied. The measured strains in the fiber are employed to estimate the position and shape of corrosion-related thinning. The pipeline test model is then used to validate the *Boundary Element Method* (BEM)-based inverse analysis algorithm. The analysis results demonstrate both accuracy and robustness of the proposed approach.

## INTRODUCTION

A reliable sensing technology and accurate numerical simulations need to be at the core of every monitoring system, as they enable management to make faster, more informed decisions. In the process, both measured and calculated quantities are used, helping to detect any undesirable changes in the monitored structure, abnormal stress and deformation patterns and/or loading conditions, leading to improvements in safety and reducing life-cycle costs.

The key component of the system is the sensor technology, which needs to ensure reliable and precise measurement results, the in-situ self-calibration, durability, and high spatial resolution. Moreover, the system must be capable of providing a large number of data, as it assists in isolating local hazards and leads to global-local analysis, and sub-structuring in numerical simulations. This is of crucial importance for large-scale, industrial applications, where parameters of interest most frequently cannot be measured directly and instead need to be estimated via inverse analysis.

The two, sometimes overlooked, essential features of the monitoring system are repeatability of the measurements and correctness of the mathematical model used in the inverse analysis procedures. The repeatability is critical in applications relying on the data-history, such as corrosion and thinning detection, where both the long-term

Neubrex Co., Ltd
Address: Hanshin-Sakae-Machi Bldg. 403A, Sakaemachi-Dori 1-1-24
650-0023 Kobe, Hyogo, Japan
E-mail: kishida@neubrex.jp

*AG on leave from Cracow University of Technology, Poland*
*YY on leave from Osaka University, Japan*

monitoring and trend analysis are used. Mathematical modeling of the physical processes always involves idealizations, i.e. simplifications, of the phenomena under consideration. However, the model must capture all of the factors relevant to the problem to yield any useful and reliable analysis results. In the pipeline thinning detection algorithms, frequently, 1D-type models are implemented. This results, at best, in underestimating depth of pipe thinning, as the uniform (averaged) thickness can be obtained, only, while the size and exact location of thinning are never detected.

In the paper, we present the robust pipe thinning detection method, built upon the *Neubrescope* fiber sensing system. The *Neubrescope* is the only commercially available high precision *Distributed Temperature and Strain Sensing* (DTSS) system, employing the *Stimulated Brillouin Scattering* (SBS). It is also capable of providing highly accurate and of cm-order spatial resolution data. The repeatability and reliability of measurements are examined in detail. The influence of polarization average, frequency-scanning step, as well as self-calibration is studied. The pipeline test model is then used to validate the *Boundary Element Method* (BEM)-based inverse analysis method. Its accuracy, convergence, and robustness are demonstrated.

## PRECISION AND REPEATABILITY OF SENSING SYSTEM

The *Neubrescope* sensing system implements the *Stimulated Brillouin Scattering* technique, and more specifically, the *Pre-Pump-Pulse Brillouin Optical Time-Domain Analysis* (PPP-BOTDA) [1, 2]. In BOTDA, two laser beams, a pump pulse and a continuous wave (CW) probe light are injected into optical fiber from both its ends. The interaction of these two laser beams excites acoustic waves, due to their different frequencies. The pump pulse is backscattered by the phonons, and part of its energy is transferred to the CW. The power gain of the CW, which is called the *Brillouin Gain Spectrum* (BGS), as a function of frequency difference between the two laser beams, is measured at the output end of the probe light while its frequency is scanned. The value of the strain/temperature can be estimated by measuring the peak frequency of the BGS, while its position along the fiber calculated from the light round-trip time (recorded by the time lag of pump laser pulse). An example of BGS distribution, resulting from one-dimensional strain state, is presented in Fig. 1.

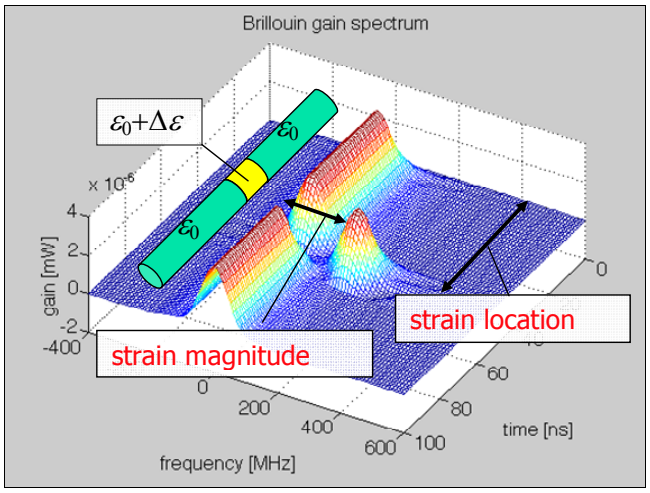


Figure 1: Strain distribution and the corresponding BGS distribution.

Naturally, the measured values of both strain location and its magnitude (see Fig. 1) are subject to errors. The quantitative and qualitative estimation of these errors are the main thrust of this and the following Section.

In the *Neubrescope* system, due to strictly designed synchronization mechanism (PXI frame), the time blur (uncertainty) of data record point is decreased to less than 10 picoseconds, what corresponds to distance blur of less than 1 mm. Table 1 summarizes all other factors influencing the accuracy and repeatability of the strain/temperature measurements.

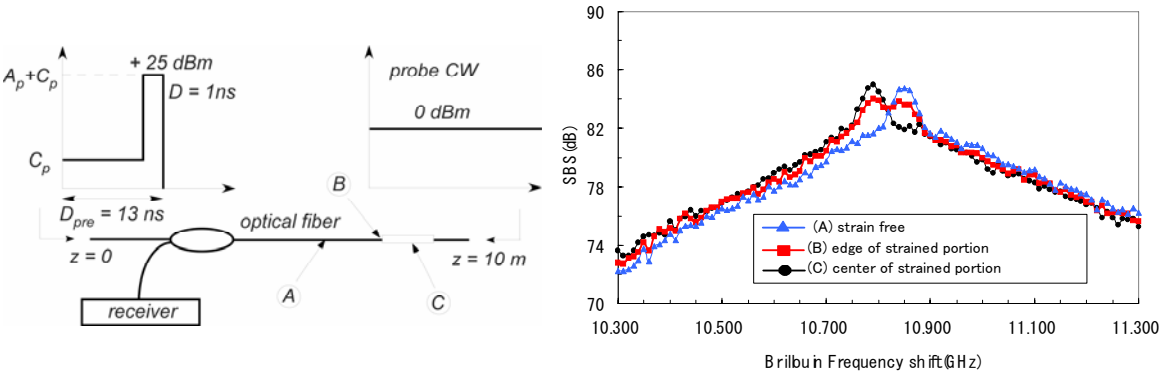


Figure 2: Example of strain distribution (1200 με) with 20 cm span.

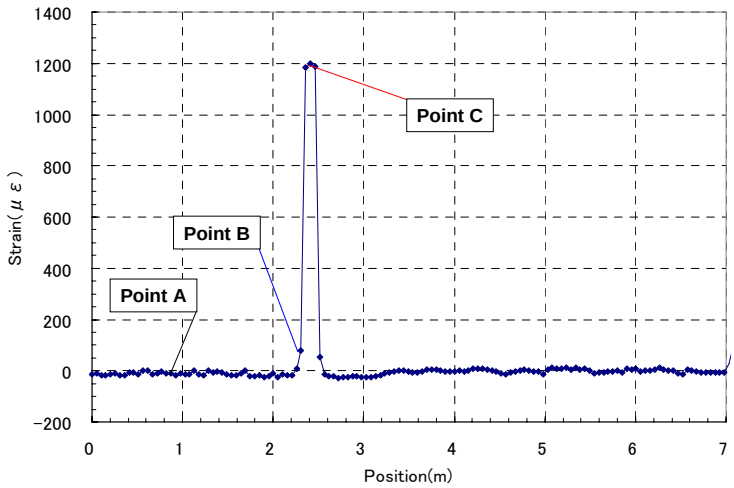


Figure 3: Strain values at points A, B, and C.

Table 1: Factors affecting accuracy and repeatability of the *Neubrescope* sensing system

| Factor | Influence on | | Source and reason |
|---|---|---|---|
| | accuracy | repeatability | |
| 1. Relative stability of the pump and probe laser | strong | strong | hardware related |
| 2. FWHM of BGS | direct | slight | 80 MHz (by design) |
| 3. S/N of BGS | direct | direct | fiber quality and settings related |
| 4. Step of frequency scanning | direct | direct | measurement time dependent |
| 5. Fitting to BGS data | slight | slight | fitting function and S/N |
| 6. Methodological error | slight | negligible | induced by PPP method |

The relative instability of the pump and probe lasers (factor 1), is mainly a result of thermal shift within electronic hardware components, and as such, can be improved only in the next generation products. Currently, it can be (hardware) controlled and decreased to ± 2.5 MHz. The *Neubrescope* system implements also the reference fiber, allowing one to calibrate the BGS peak frequency, further reducing the instability to just 0.7 MHz. The Full Width at Half Maximum (FWHM) (factor 2) is set in *Neubrescope* by design to 80 MHz. Factor 3, namely, the signal-to-noise ratio (S/N) can be improved mainly by increasing the number of averages. The estimation of its value on the measured strain is listed in Table 2.

Table 2: Number of averages and its influence on repeatability

| No. of averages | Frequency step | Repeatability |
|---|---|---|
| $10^{13}$ | 5 MHz | ±2.5 MHz (± 50 με) |
| $10^{14}$ | 5 MHz | ±2.1 MHz (± 42 με) |
| $10^{15}$ | 5 MHz | ±1.8 MHz (± 36 με) |

Factors 4 and 5 (Table 1), that is, both step of frequency scanning and BGS data fitting, can be significantly improved by decreasing the step size (i.e. from 10 to 5 MHz). However, due to influence of pump and probe laser instability (factor 1), it will bring no effect for steps below 1 MHz. The methodological error, introduced by the PPP method itself, depends on the specific strain pattern but in any case, it does not exceed 25 με.

## EXAMINATION OF REPEATABILITY AND ITS CHARACTERISTICS

The theoretical estimation of measurement repeatability and uncertainties, presented in the previous Section, was validated with a series of experimental tests. One of the experimental stands used is shown in Fig. 4.


Figure 4: Specimen for thinning detection test.

During this particular experiment, the strain at the external surface of the pipe was measured 5 times. The measurement results are presented in Fig. 5, where the upper portion shows the absolute values, while the lower the differences between all measured strains.

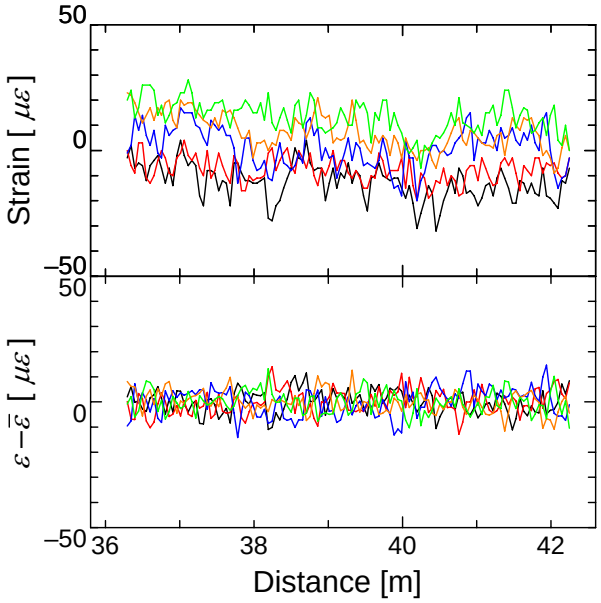


Figure 5: Results of five consecutive measurements with the same setting (average $10^{13}$, frequency step 5MHz)

Table 3: Estimated repeatability according to measurement settings

| No. of averages | Frequency scanning step | Design | | Experiment |
|---|---|---|---|---|
| | | frequency | strain | |
| [-] | [MHz] | [MHz] | [± με] | [με] |
| $2^{13}$ | 10 | 5.0 | 100 | 23 |
| | 5 | 2.5 | 50 | 14 |
| | 2 | 1.0 | 20 | 6 |
| | 1 | 0.5 | 10 | 3 |
| $2^{14}$ | 10 | 4.2 | 84 | 20 |
| | 5 | 2.1 | 42 | 12 |
| | 2 | 0.84 | 17 | 7.5 |
| | 1 | 0.42 | 8.5 | 3 |
| $2^{15}$ | 10 | 3.5 | 70 | 17 |
| | 5 | 1.8 | 35 | 7.8 |
| | 2 | 0.7 | 14 | 4 |
| | 1 | 0.25 | 7 | 2 |

The Gaussian distribution (with zero mean value) is obtained, what clearly demonstrates that the instrument is properly designed. The standard deviation of 14 με is achieved. Taking into account that the errors listed in Table 2 are the maximum errors of 3σ, the experimental results are in a very good agreement with theoretical values.

The estimation of uncertainties for a wider range of hardware settings is summarized in Table 3, where the already verified values are in red color. The uncertainty as small as 7 με were also achieved. The presented analysis and experimental test demonstrate that the *Neubrescope* optical sensing system can be employed for high-precision strain and/or temperature monitoring.

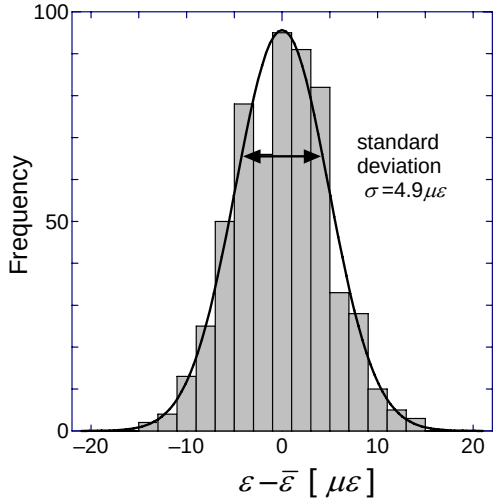


Figure 6: Errors distribution (*Neubrescope* NBX-6000)

## APPLICATION EXAMPLE

This Section includes the benchmark test, validating the derived inverse analysis algorithm and demonstrating its robustness. Example deals with the thinning detection problem within a portion of pipeline.

The geometrical configuration of the analyzed domain and the optical fiber location were kept as in the experimental test presented in [3], with the following dimensions used: pipe external diameter of 300 mm, pipe thickness of 10 mm, and the total length of 1000 mm. As thermophysical properties, the constant values were assumed, namely: modulus of elasticity 3.3 GPa, and Poisson's ratio 0.35. The internal pressure was assumed to be as high as 1.0 MPa. The BEM mesh comprised of 2112 surface quadrilateral elements. The BEM formulation employed in this study included the *nearly singular integration* procedures [4], which were required due to small thickness of the analyzed domain.

The sought for thinning was parameterized by assuming that its area was circular-shaped. Parameterization brought a desired effect of reducing the number of unknowns. Two inverse models were considered, namely, with two- and four-parameters. In two-parameter model, the unknown were size and depth of the thinning, only, while the more realistic four-parameters model accounted for size, depth and position in both circumferential and axial directions of the thinning.

First, the forward structural problem was solved (with assumed shape and location of the pipe thinning). The values of strain tensor were transformed to fiber strain, imposing the uniform weighting function in the moving average [1] algorithm, yielding simulated and noise-free strain data (see Fig. 7a). The two small peaks of strain value were produced by optical fiber located at the edge of the circular-shaped thinning area, while the distinguishable (highest) strain peak by one passing directly over the thinning area.

The implemented inverse analysis procedure used a series of BEM forward solutions to obtain the sensitivity coefficients and form the Jacobian matrix, e.g. [5]. As the problem under consideration was non-linear (the sensitivity matrix elements were shape-dependent), the solution was obtained iteratively. The BEM-based formulation

enabled one to easily and quickly update (remesh) the boundary of the domain. At each iteration step, only a small number of the BEM *influence matrices* entries needed to be modified, making the procedure numerically very efficient. Moreover, the convergence rate of the inverse procedure was very high, as clearly shown in the Fig. 7b, allowing one to achieve the final solution in just a few steps.

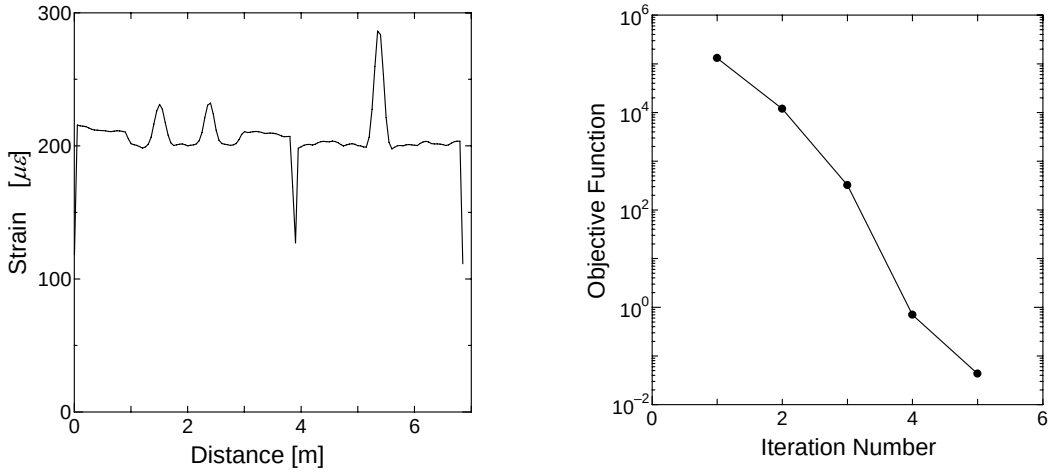


Figure 7: Simulated strain distribution in the optical fiber (left) and convergence (right)

Next, in order to verify the stability of the solution algorithm, the measurement errors were imposed on the data. Several levels of noise were considered here, all guided by the repeatability analysis presented in the foregoing Section. For each analyzed noise level, up to 15 different data cases (problems) were generated. The selected measurement data is presented in Fig. 8.

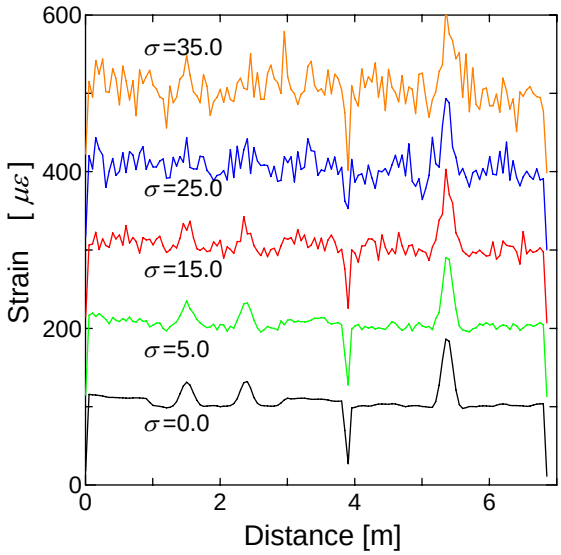


Figure 8: Strain distribution in the optical fiber with different noise level σ [με]

The strains measured at the edge of the thinning area, were now buried under the data noise, and could not be as easily distinguished as it was in the noise-free case. Despite that, the achieved solution results confirmed the high accuracy and robustness of the derived algorithm. The selected results are listed in Table 4 and 5, where target values were (150, 5.0) and (150, 5, 3.14, 0.5), respectively.

Table 4: Estimation results – 2 parameters and measurement uncertainty ± 25.0 με

| Case ID | Estimated thinning | | Objective function | Iterations |
|---|---|---|---|---|
| | radius | depth | | |
| 11 | 134.794 | 5.536 | 14.227 | 6 |
| 12 | 144.291 | 4.957 | 13.619 | 5 |
| 13 | 142.126 | 5.303 | 13.333 | 5 |
| 14 | 146.818 | 4.681 | 13.828 | 5 |
| 15 | 153.149 | 4.256 | 13.791 | 5 |

Table 5: Estimation results – 4 parameters and measurement uncertainty ± 25.0 με

| Case ID | Estimated thinning | | | | Objective function | Iterations |
|---|---|---|---|---|---|---|
| | radius | depth | hoop | axial | | |
| 11 | 135.983 | 5.472 | 3.140 | 0.505 | 14.221 | 12 |
| 12 | 142.627 | 5.066 | 3.142 | 0.520 | 13.464 | 7 |
| 13 | 143.416 | 5.247 | 3.121 | 0.493 | 13.285 | 10 |
| 14 | 146.816 | 4.684 | 3.121 | 0.499 | 13.822 | 8 |
| 15 | 146.538 | 4.656 | 2.914 | 0.496 | 13.426 | 7 |

## CONCLUSIONS

In this paper, we presented the robust pipe thinning detection method. The algorithm utilized the *Neubrescope* optical fiber sensing system, providing the strain data. The accuracy and reliability of the system were analyzed in detail. In all examined cases, the desired Gaussian error distribution was observed. The measured strains were used to estimate the shape, size, and location of the corrosion-based thinning of the pipeline via BEM-based inverse analysis method. Its accuracy, convergence, and robustness were demonstrated.

## REFERENCES


1. K. Kishida, C-H. Li, K. Nishiguchi. Pulse pre-pump method for cm-order spatial resolution of BOTDA, *17th International Conference on Optical Fiber Sensors*, (Editors: Sensors, M. Voet, R. Willsch, W. Ecke, J. Jones, B. Culshaw). *SPIE*, pp.559-562. (2005)
2. K. Kishida, C-H. Li. Pulse pre-pump-BOTDA technology for new generation of distributed strain measuring system, *Structural Health Monitoring and Intelligent Infrastructure*, (Editors: Ou, Li, Daun). *Taylor & Francis*, pp.471-477. (2006)
3. K. Kishida, H. Zhang, C-H. Li, A. Guzik, H. Suzuki, Z. Wu. Diagnostic of corrosion based thinning in steam pipelines by means of Neubrescope high precision optical fiber sensing system, *in Proceedings of The 5th International Workshop on Structural Health Monitoring, Stanford University, Stanford, USA*, (Editor: F-K Chang). *DEStech Publications, Inc.*, pp.1363-1370. (2005)
4. T. Matsumoto, A. Guzik, M. Tanaka. Some transformation methods for evaluation of nearly singular integrals and their applications to BEM analyses of thin-shell structures. *Transactions of JASCOME*, 5, 195-200. (2005)
5. I. Nowak, A. J. Nowak, L. C. Wrobel. Inverse analysis of continuous casting processes, *The International Journal of Numerical Methods for Heat & Fluid Flow*, Vol. 13 (5), pp. 547-564. (2003)